Models for saccadic motion and postsaccadic oscillations

J. A. Del Punta,[1,2] K. V. Rodriguez,[1,3] G. Gasaneo,[1,3] and S. Bouzat[4,*]

[1]*Neufisur-Departamento de Física, Universidad Nacional del Sur-IFISUR, (8000) Bahía Blanca, Argentina*

[2]*Departamento de Matemática, Universidad Nacional del Sur, (8000) Bahía Blanca, Argentina.*

[3]*CINA-Centro Integral de Neurociencias Aplicadas, (8000) Bahía Blanca, Argentina*

[4]*Centro Atómico Bariloche (CNEA), Consejo Nacional de Investigaciones Científicas y Técnicas, Av. E. Bustillo 9500 R8402AGP San Carlos de Bariloche Río Negro, Argentina*

(Received 26 October 2018; published 29 March 2019)

In a recent letter [S. Bouzat *et al.*, Phys. Rev. Lett. **120**, 178101 (2018)], a mathematical model for eyeball and pupil motion was developed allowing for the understanding of the postsaccadic oscillations (PSO) as inertial effects. The model assumes that the inner part of the iris, which defines the pupil, moves driven by inertial forces induced by the eyeball rotation, in addition to viscous and elastic forces. Among other achievements, the model correctly reproduces eye-tracking experiments concerning PSO profiles and their dependence on the saccade size. In this paper we propose various extensions of the mentioned model, we provide analytical solutions, and we perform an exhaustive analysis of the dynamics. In particular, we consider a more general time dependence for the eyeball velocity enabling the description of saccades with vanishing initial acceleration. Moreover, we give the analytical solution in terms of hypergeometric functions for the constant parameter version of the model and we provide particular expressions for some cases of interest. We also introduce a new version of the model with inhomogeneous viscosity that can improve the fitting of the experimental results. Our analysis of the solutions explores the dependence of the PSO profiles on the system parameters for varying saccade sizes. We show that the PSO emerge in critical-like ways when parameters such as the elasticity of the iris, the global eyeball velocity, or the saccade size vary. Moreover, we find that the PSO profiles with the first overshoot smaller than the second one, which are usually observed in experiments, can be associated to parameter regions close to criticality.

DOI: 10.1103/PhysRevE.99.032422

I. INTRODUCTION

When we look at a picture or a face, our gaze scans the image not in a spatially continuous way but by performing a succession of *jumps* between relatively distant points. Each of these jumps or gaze shifts is called a *saccade* and involves a fast coordinated rotation of the eyeballs that changes the fixation point [1–3]. The duration of a saccade is typically of the order of 100–200 ms, while the saccade amplitudes (from here on referred to as saccade's sizes) range from less than 1° to 30° or more.

Together with the progress of modern eye-tracking techniques [3], which on a yearly basis provide simpler ways of registering the eye movements, the analysis of saccadic motion is becoming a common practice in many areas of science, particularly in psychology and neuroscience, and also in industry, marketing, and games [3]. In this context, the development of mathematical models that allow us to understand different aspects of eye motion has called the attention of physicists, mathematicians, and engineers in recent years. In particular, within the area of interdisciplinary physics, relevant contributions have been made concerning the dynamics of saccades [4–9], microsaccades [10,11], and fixation [12,13]. This paper continues the developments in Ref. [9] concerning pupil and eyeball dynamics during saccades, which, in turn, added physical considerations to previous advances on the modeling of sacaddic motion [6].

Typical signals recorded by eye trackers show that, at the end of a saccade, before the steady regime corresponding to the fixation, the pupil signal usually performs a damped oscillation with one or two observable periods before complete damping. These are the so called postsaccadic oscillations (PSO) [14,15]. The maximal amplitudes of the PSO are normally in the range 0–2° and their periods are of the order of 20 ms [15].

Recently, the origin of the PSO has been related to dynamical deformations of the internal border of the iris during sacaddes [14–16] or, in other words, with the motion of the pupil inside the eyeball. This is the so called *iris wobbling* or *eye wobbling* phenomenon [17,18] prompted by relative movements between internal parts of the eye during saccades. The PSO profiles vary among individuals [15,19] and change with the age of the observer [19]. Moreover, they also depend on the direction of the saccade [15] and are influenced by the pupil size [20] and by the eye tracking technique used [16,19,21].

In the recent letter of Ref. [9], some of us and other collaborators have proposed a two-variable mathematical model for the motion of the eyeball and the relative position of the center of the pupil during saccades. The model allowed us to reproduce the dependence of the PSO profiles on the saccade size recently reported in Ref. [15], and also to relate such a dependence to that of the peak velocity, which was measured

*bouzat@cab.cnea.gov.ar.

in independent experiments [22,23] (see also experiments in Refs. [6,19]). According to our model, the PSO are damped harmonic oscillations induced by the inertial forces associated to the eyeball deceleration at the end of the saccade. Such inertial forces act effectively on the inner part of the iris and possible on other internal pieces of the eye. The oscillations are influenced by the viscoelastic characteristics of the medium. For the sake of shortness, we refer to the dynamics of the center of the pupil during saccades as the pupil motion or pupil dynamics.

The model developed in Ref. [9] arises as a powerful and easy-to-handle tool for analyzing saccade and PSO dynamics, and for giving a physical interpretation of the experimental data. Moreover, the results in Ref. [9], together with the ideas and experimental evidences provided in Refs. [14–16,19], strongly suggest that the analysis of the PSO can open a door to characterize the internal structure of the eye and its mechanical properties. This has an interesting parallel to the fact that, in a wider time scale, the analysis of sequences of saccades helps to characterize psychological and neurological conditions.

The purpose of this paper is twofold. First, we provide analytical solutions for the model developed in Ref. [9] considering a more general functional form for the force that drives the eyeball rotation. Second, we perform a detailed physical analysis of the solutions for eyeball and pupil motion for varying parameters. The analysis includes results for a new version of the model that considers space dependent viscoelastic properties [9]. Hence, this work generalizes in various ways the model proposed in Ref. [9], provides analytical solutions and expands the dynamical analysis considerably.

The paper is organized as follows. In Sec. II we present the model introduced in Ref. [9] and we explain the generalizations considered. In Sec. III we review the main results in Ref. [9] and we dwell deeper in some of the objectives of the present work. In Sec. IV we present the analytical solutions for the constant parameters version of the model. In Secs. V–VII we perform the physical analysis of the solutions for eyeball and pupil motion considering different model versions and conditions. Section VIII is devoted to the conclusions.

II. MODEL FOR EYEBALL AND PUPIL MOTION DURING SACCADES

Here we revisit the one-dimensional model for saccadic motion proposed in Ref. [9] and we introduce the new ingredients and generalizations considered.

The model has two dynamical variables. Namely, $x(t)$, that describes the angular displacement of the eyeball along a saccade, and $y(t)$, that stands for the relative position of the pupil inside the eyeball. More precisely, $x(t)$ can be considered as the angular position of the center of the cornea in a rigid description of the eyeball (i.e., disregarding the fact that the cornea may deform during the saccade). Meanwhile, $y(t)$ represents the angular displacement of the center of the pupil with respect to $x(t)$ in the direction of the saccade. In this way, the *absolute* position of the center of the pupil along a saccade, to be compared for instance with data taken from an eye tracker signal, is given by $x(t)+y(t)$.

To define the dynamics of $x(t)$ we assume that the eyeball motion is driven by the extra ocular muscles in an overdamped way [24]. Hence, we have the simple equation

$$\nu\,\dot{x} = F(t). \tag{1}$$

Here, ν is the viscosity constant acting on the eyeball and $F(t)$ is the force produced by the extra ocular muscles. For simplicity we fix $\nu = 1$ so that $F(t)$ is scaled with the viscosity.

Given that Eq. (1) has translational symmetry on x and that we are only interested in describing single saccades, we consider the initial condition $x(0) = 0$ with no loss of generality. The anisotropies and inhomogeneities that may affect the eyeball motion on different directions or regions of the visual field can be taken into account by varying characteristics of $F(t)$.

The model assumes that the iris is elastically linked to the eyeball and that, when the eyeball rotates, the iris itself and also other internal parts of the eye linked to it (such as the lens) suffer inertial forces induced by the eyeball motion. The main assumption is that, due to this, the internal border of the iris (which defines the pupil) oscillates in such a way that the center of the pupil behaves effectively as a point particle subject to inertial forces on the reference frame of the eyeball. Thus, the dynamical equation considered is

$$\ddot{y} + \gamma\,\dot{y} + k\,y = -\ddot{x}. \tag{2}$$

Here, k is the effective elastic constant for the force $-ky$, which tends to align the center of the pupil with the center of the cornea, while γ measures an effective viscosity affecting the relative motion. Finally, $-\ddot{x}$ stands for the inertial force *felt* by the pupil in the reference frame of the eyeball. Note that the mass is set equal to 1 with no loss of generality. The units of k, γ, and $F(t)$ can be chosen to express x and y in degrees and time in milliseconds. The initial conditions considered are $y(0) = 0$ and $\dot{y}(0) = 0$ so that the pupil is at rest at its relaxation position on the eyeball, which coincides with the center of the cornea.

In this work we consider the forcing as given by

$$F(t) = A\,t^{\beta}\,\exp\left[-\frac{t^{\mu}}{\tau^{\mu}}\right], \tag{3}$$

where $A > 0$, $\mu > 0$, $\beta \geqslant 1$, and $\tau > 0$ are parameters that control the shape and size of the saccade in a way that we analyze below. This proposal generalizes the formula considered in Ref. [9], which corresponds to the case $\beta = 1$. The analysis in [9] was also limited to the case $\mu = 2$, while below we address the influence of μ on the saccade and PSO shapes.

Regarding the role of the parameter β, note that by expanding Eq. (3) for small t we get $F(t) \simeq At^{\beta} + o(t^{\beta+\mu})$. Then, Eq. (1) leads to $\dot{x}(t) \simeq At^{\beta}$ at short times, and $\ddot{x}(t) \simeq A\beta t^{\beta-1}$. This shows that the case $\beta < 1$ (not considered) is physically meaningless since it leads to an infinite initial acceleration and thus invalidates the overdamped approximation. Moreover, we see that the initial acceleration coincides with the parameter A for $\beta = 1$ and vanishes for $\beta > 1$.

While the parameters A, μ, β, and τ determine the forcing profile acting on the eyeball (i.e., they could be fitted to reproduce the activity of the extra ocular muscles), the parameters γ and k characterize the viscoelastic properties

of the iris-eyeball link concerning the relative motion of the pupil. Along this work, we analyze basically three different proposals for these parameters. The simplest one considers k and γ as constants and independent of the saccade size. This approach, referred to as *model with constant parameters*, is good enough to understand the basic phenomenology of the PSO, including for instance the dependence of the PSO amplitude and period on the saccade size, as shown in Ref. [9]. However, accurate fitting of families of saccades of different sizes performed by the same eye may require to consider the viscoelastic properties of the iris as non constant. We thus propose two alternative versions of the model. The first one, referred to as *model with force dependent parameters*, considers the parameters k and γ as functions of $F(t)$. This model was briefly analyzed in Ref. [9]. The idea underlying this assumption is that the action of the muscles that rotate the eyeball may also produce smooth deformations which can change the interaction between the iris and other internal parts of the eye. The second one corresponds to a model *with inhomogeneous viscosity* that considers γ as dependent on $y(t)$. Finally, we also discuss the possibility of considering the model with constant parameters but with values adaptable for each saccade size.

III. PREVIOUS RESULTS AND RELATION TO EXPERIMENTS

In this section we briefly review some of the main results of Ref. [9] and we dwell deeper in the objectives of the present work.

In Ref. [9], the model with $\mu = 2$ and $\beta = 1$ was solved numerically to reproduce and interpret previous experimental findings on saccadic motion and PSO behavior. It was first shown [9] that the model produces saccades and PSO profiles for pupil motion compatible with experiments. Examples of the saccades generated are depicted here in Figs. 1(a) and 1(b). As mentioned in the Introduction, by PSO we refer to the oscillations observed at the end of the saccade, that typically begin with an overshoot. It is worth stressing that we consider the PSO as part of the saccade profile, that finishes when the curve attains its asymptotic value [see the caption of Fig. 1(b)]. In Ref. [9] it was also shown that, by considering a fixed value of A and varying only the parameter τ to fit the the desired saccade size x_m, the eyeball maximal velocity $\mathrm{Max}[\dot{x}(t)]$ obtained with the model is proportional to $x_m^{1/2}$. Then, the peak velocity of the pupil $\mathrm{Max}[\dot{x}(t) + \dot{y}(t)]$, which is essentially determined by this law [as shown in Fig. 1(c)],

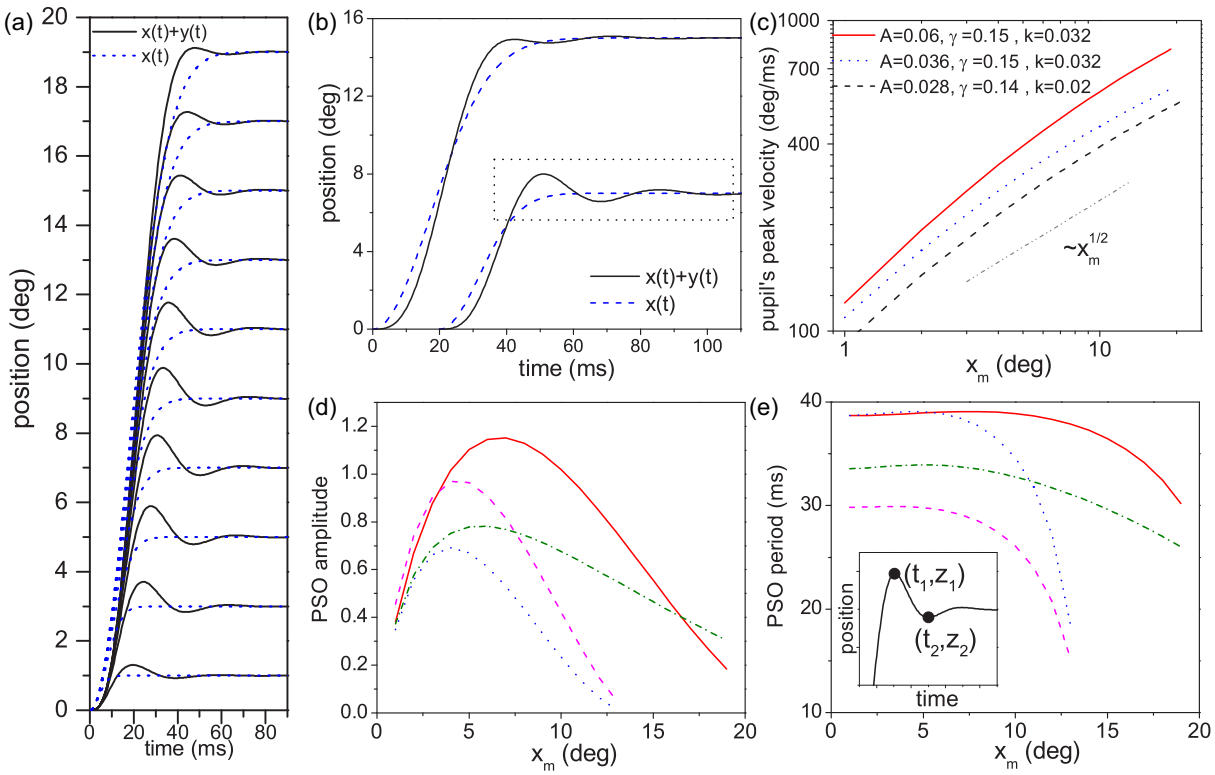

FIG. 1. Summary of previous results for saccades and PSO with $\beta = 1$ and $\mu = 2$. (a) Eyeball $[x(t)]$ and pupil $[x(t) + y(t)]$ motion for the family of saccades with constant $\mu = 2$, $A = 0.06$, $\gamma = 0.15$, $k = 0.032$ for varying x_m. (b) Detail of eyeball and pupil positions during saccades of sizes $x_m = 7$ and $x_m = 15$ calculated for $A = 0.05$, $\gamma = 0.1$, $k = 0.035$. The timescale for the saccade with $x_m = 7$ is shifted for the sake of clarity. The dotted rectangle indicates the PSO domain for the saccade with $x_m = 7$. (c) Pupil's peak velocity vs x_m. The red solid line, the blue dotted line and the black dashed one correspond to families of saccades with constant μ, β, A, γ, and k for the values indicated. The dash-dot-dotted line shows the $x_m^{1/2}$ behavior for reference. (d) Amplitude of the PSO as a function of x_m. The red solid line, the blue dotted line and the green dash dotted line are for the same calculations in panel (c), with corresponding line types. The pink dashed line is for $A = 0.06$, $\gamma_0 = 0.15$, $k_0 = 0.05$. (e) Period of the PSO as a function of x_m for the same calculations in panel (d), with corresponding line types. The inset sketches the method for calculation of amplitude and period of the PSO using the position of the first overshoot. The amplitude is defined as $z_1 - z_2$, while the period is $2(t_2 - t_1)$. In all the panels, all calculations are for $\mu = 2$, $\beta = 1$.

results in close agreement with well known experiments [6,22,23]. These results showed the convenience of considering x_m as a relevant system parameter instead of τ. For $\mu = 2$ and $\beta = 1$ we have the simple relation $\tau = \sqrt{2x_m/A}$ [9], while the general relation is presented below in Eq. (6).

Then, it was found that, by keeping fixed values of A, k, and γ and varying only x_m (i.e., varying τ), the model produces saccades of different sizes for which the dependence of the PSO profiles on x_m are in good qualitative agreement with the experimental findings in Ref. [15] (in addition to provide correct results for the peak velocity). As Figs. 1(a) and 1(d) show, the PSO amplitude grows with x_m for small x_m, then it attains a maximum at a value of x_m in the range 5–8°, and finally it decreases with x_m [15]. Eventually, the PSO can be suppressed at large x_m [15], depending on the parameters. Meanwhile, the PSO period is essentially constant (or slightly increasing) for $x_m \lesssim 5°$ and it decreases for larger values of x_m [see Fig. 1(e)], as observed in experiments in Ref. [15]. Note that the inset in Fig. 1(e) sketches the way in which the PSO amplitude and period are calculated according to the explanation given in the caption.

The fact that the model reproduces these behaviors clearly supports the ansatz in Eq. (3) and the model as a whole, and strongly suggests that the PSO are mainly ruled by inertial effects. The results indicate that the dependence of the PSO profiles on x_m is intimately related to that of the peak velocity. Note that, before the developments in Ref. [9], the experimental results for the amplitude and period of the PSO in Ref. [15] could have been thought as completely independent of those for the peak velocity obtained in Refs. [6,22,23].

To obtain the mentioned experimental findings concerning PSO profiles and dependence on x_m, the authors of Ref. [15] analyzed saccades from various observers (and eyes) obtained when performing the simple task of moving the gaze between two points separated (horizontally or vertically) by a certain angle. Importantly, as two saccades profiles obtained from the same eye when performing the same task are in general different each other [15], the experiments actually report *families of averaged saccades*. Each family corresponds to an eye and to a fixed direction (e.g., upward, downward, left, etc.). Meanwhile, each averaged saccade of the family corresponds to a different saccade size [15]. As part of our work, we investigate the role of the model parameters in determining the saccade and PSO profiles within a family. On the base of the mentioned previous theoretical findings, our first assumption to generate a family of saccades will be to keep the parameters A, μ, β, k, and γ fixed, and change only x_m. However, we also discuss other possibilities.

Although in this paper we focus on the general analysis of the solutions of the model and not on fitting particular experiments, it is important to mention that the PSO profiles can strongly depend on the eye tracker technique, and the model parameters could need to be adapted to different experiments. In particular, in Ref. [16] it was shown that pupil-corneal reflection signals (p-CR) recorded in p-CR eye trackers (conceived to compensate small motions of the head of the observers) differ from pupil (p) signals. The amplitudes of the PSO are considerably larger in p-CR signals. In the Supplemental Material to Ref. [9], it was shown that if $x(t) + y(t)$ models the p signal, the p-CR signal can be approximated as $x(t) + \lambda y(t)$ with $\lambda \sim 2$. This point requires, however, further analysis and a detailed modeling of the corneal reflection signal to be completely clarified. Nevertheless, although our model is conceived to describe the p signal, the dynamics of $x(t) + y(t)$ could also be used to fit p-CR signals without the inclusion of the factor λ [9]. As indicated in Ref. [9], in such case, the parameters k and γ should not be interpreted as those associated directly to the pupil motion.

IV. ANALYTICAL SOLUTIONS

The studies in Ref. [9] were based on numerical solutions. The only analytical solution provided was the one for $x(t)$ considering $\mu = 2$ and $\beta = 1$. Here we give the general solution for $x(t)$ for arbitrary values of μ and β, and we also present the complete solution for $y(t)$ for the model with constant parameters.

A. Analytical solution for the eyeball motion

Using the force given in Eq. (3) and the condition $x(0) = 0$, the trajectory $x(t)$ can be integrated from Eq. (1) to get

$$x(t) = A\frac{t^{\beta+1}}{\beta+1}\,{}_1F_1\left[\frac{\beta+1}{\mu}, \frac{\beta+\mu+1}{\mu}; -\left(\frac{t}{\tau}\right)^{\mu}\right], \tag{4}$$

where ${}_1F_1(a, b, z)$ is the Kummer function [25,26] (see the Appendix for a definition of the Kummer function and of other special functions used). For large t, the Kummer function behaves as $\sim\Gamma(\frac{\beta+\mu+1}{\mu})(\frac{\tau}{t})^{\beta+1}$. Thus, the long time limit of $x(t)$, which corresponds to the saccade size x_m, yields

$$x_m \equiv \lim_{t\to\infty} x(t) = A\frac{\tau^{\beta+1}}{\beta+1}\Gamma\left(\frac{\beta+\mu+1}{\mu}\right). \tag{5}$$

As explained in the previous section, it is convenient to consider x_m as a relevant system parameter instead of τ. The explicit relation is obtained by inverting Eq. (5):

$$\tau = \left(\frac{(\beta+1)x_m}{A\,\Gamma\left(\frac{\beta+\mu+1}{\mu}\right)}\right)^{\frac{1}{\beta+1}}. \tag{6}$$

Although in our analysis of the dynamics we will focus on the role of x_m, for the sake of shortness we keep on using the parameter τ to present the solutions. Note, for instance, that the solution for $x(t)$ in terms of the parameters A, μ, β and x_m is obtained by replacing τ from Eqs. (6) in (4).

The maximal eyeball velocity can be shown to occur at $t = \tau(\beta/\mu)^{1/\mu}$ and yields $\mathrm{Max}[\dot{x}] = A\tau^{\beta}(\beta/\mu)^{\beta/\mu}e^{-\beta/\mu}$. In terms of x_m this can be expressed as

$$\mathrm{Max}[\dot{x}] = \mathcal{C}(A, \mu, \beta)\, x_m^{\frac{\beta}{\beta+1}}, \tag{7}$$

with

$$\mathcal{C}(\mu, \beta, A) = A\left(\frac{\beta+1}{A\Gamma\left(\frac{\beta+\mu+1}{\mu}\right)}\right)^{\frac{\beta}{\beta+1}}\left(\frac{\beta}{\mu}\right)^{\frac{\beta}{\mu}}e^{-\frac{\beta}{\mu}}. \tag{8}$$

Note that, for a family of saccades generated at fixed values of A, μ, and β, Eq. (7) predicts a power-law dependence for $\mathrm{Max}[\dot{x}]$ on the saccade size with an exponent $\beta/(\beta+1)$ (i.e., independent of A and μ). This generalizes the findings in Ref. [9] for $\beta = 1$, that led to an exponent $1/2$. As mentioned

before, the dependence of $\mathrm{Max}[\dot{x}(t)]$ on x_m strongly influences that of the peak velocity of the pupil $\mathrm{Max}[\dot{x}(t)+\dot{y}(t)]$, which is the relevant quantity to be compared with experiments. In fact, although the exponent for $\mathrm{Max}[\dot{x}(t)+\dot{y}(t)]$ results smoothly dependent on x_m [9], it is expected to be close to that for $\mathrm{Max}[\dot{x}(t)]$ throughout the relevant range of x_m [9]. Meanwhile, the exponents found in the experiments of Refs. [6,19,22,23] vary for different observers, directions of the saccade, and also depend smoothly on x_m, but they seem to be always roughly in the range 0.4–0.75. This suggests that values of $\beta > 1$ in the range 1–1.3 (approximately) may be of interest. Finally, we recall that the results for $\beta = 1$ obtained in Ref. [9] suggest $1.5 \lesssim \mu \lesssim 4$ and $0.02 \lesssim A \lesssim 0.06$ as the relevant ranges for the remaining parameters.

For the case $\beta = 1$, the solution in Eq. (4) has the following alternative expression in terms of x_m,

$$x(t) = x_m - \frac{At^2}{\mu}\mathrm{Ei}\left[\frac{\mu-2}{\mu}, t^{\mu}\left(\frac{A\Gamma\left(\frac{\mu+2}{\mu}\right)}{2x_m}\right)^{\mu/2}\right], \tag{9}$$

where $\mathrm{Ei}(n,z)$ is the exponential integral function (see Appendix). For $\mu = 2$, this reduces to the simple expression $x(t) = x_m(1-\exp[-\frac{At^2}{2x_m}])$ presented in Ref. [9].

B. Analytical solution for the pupil motion with constant parameters

Here we present the exact solution for $y(t)$ for the case of constant values of γ and k. The reader interested mainly in the dynamical aspects of the model and not in the mathematical details of the solution may skip this subsection, knowing, however, that the analytical solution for $y(t)$ is given in Eq. (15).

By combining Eqs. (1) and (2), the equation for $y(t)$ results in a standard forced harmonic oscillator,

$$\ddot{y}(t) + \gamma\dot{y}(t) + ky(t) = -F'(t), \tag{10}$$

with the forcing $-F'(t)$ defined [according to Eq. (3)] through

$$F'(t) = Ae^{-(t/\tau)^{\mu}}\left(\beta t^{\beta-1} - \frac{\mu}{\tau^{\mu}}t^{\beta+\mu-1}\right). \tag{11}$$

Taking into account that, for $\beta \geqslant 1$, $F'(t)$ is finite at $t = 0$, the particular solution satisfying the initial conditions $y(0) = y'(0) = 0$ can be written as

$$y(t) = -\int_0^t dt' G(t,t')\,F'(t'), \tag{12}$$

where $G(t,t')$ is the sinusoidal Green's function

$$G(t,t') = \begin{cases} 0, & \text{if } t-t' < 0, \\ \frac{1}{\Omega}e^{-\gamma(t-t')/2}\sin[\Omega(t-t')], & \text{if } t-t' > 0. \end{cases} \tag{13}$$

Note that, considering the context of complex variables, the formula in Eq. (12) holds (and gives a real number) regardless of the sign of $k-\gamma^2/4$, and it is also valid in the limit $\Omega \to 0$.

Now, setting $\alpha^{(\pm)} = \gamma/2 \pm i\Omega$ and defining

$$I_{\mu}(\alpha^{(\pm)}, \beta, \tau; t) = \int_0^t ds\, s^{\beta}\, e^{\alpha^{(\pm)}s}\, e^{-(s/\tau)^{\mu}}, \tag{14}$$

we obtain

$$\begin{aligned} y(t) = &-\frac{A\beta}{2i\Omega}[e^{-\alpha^{(-)}t}I_{\mu}(\alpha^{(-)}, \beta-1, \tau; t) - e^{-\alpha^{(+)}t}I_{\mu}(\alpha^{(+)}, \beta-1, \tau; t)] \\ &+\frac{A\mu}{2i\Omega\tau^{\mu}}[e^{-\alpha^{(-)}t}I_{\mu}(\alpha^{(-)}, \beta+\mu-1, \tau; t) - e^{-\alpha^{(+)}}I_{\mu}(\alpha^{(+)}, \beta+\mu-1, \tau; t)]. \end{aligned} \tag{15}$$

By expanding the factor $e^{-(s/\tau)^{\mu}}$ in Eq. (14) in power series and expressing the resulting integral in terms of Kummer functions [25], the integral $I_{\mu}(\alpha^{(\pm)}, \beta, \tau; t)$ can be expressed as

$$I_{\mu}(\alpha^{(\pm)}, \beta, \tau; t) = t^{\beta+1}\, e^{\alpha^{(\pm)}t}\sum_{n=0}^{\infty}\frac{(-1)^n}{n!}\left(\frac{t}{\tau}\right)^{\mu n}\frac{1}{\beta+\mu n+1}\,{}_1F_1(1, \beta+\mu n+2; -\alpha^{(\pm)}t). \tag{16}$$

For $\mu = 2$, the function $I_{\mu}(\alpha, \beta, \tau; t)$ has an alternative expression given by

$$I_2(\alpha, \beta, \tau; t) = \frac{t^{\beta+1}}{\beta+1}\sum_{n=0}^{\infty}\frac{(\beta+1)_n}{(\beta+2)_n}\frac{(\alpha t)^n}{n!}\,{}_1F_1\left(\frac{\beta+1+n}{2}, \frac{\beta+3+n}{2}; -\frac{t^2}{\tau^2}\right). \tag{17}$$

Here, $(z)_n = \Gamma(z+n)/\Gamma(z)$ is the Pochhammer symbol [25]. Equation (17) resulted useful for evaluating the solution $y(t)$ in the relevant case $\mu = 2$ considered in most of our studies. The convergence properties of the series appearing in Eqs. (16) and (17) can be obtained with relative ease. Although the mathematical details are out of the scope of this paper, we can mention some of the steps. First, the factor $\frac{1}{\beta+\mu n+1}$ can be transformed into a quotient of Pochhammer symbols as the one appearing on Eq. (17). Second, by expanding in power series the Kummer function on any of the equations, we can obtain a two-variable hypergemetric function. The numbers of Pochhammer symbols in the numerator and in the denominator allow us to ensure, taking into account the developments in Ref. [27], that the series converges.

V. EYEBALL DYNAMICS

Here we analyze the model predictions for the eyeball motion and the role of the parameters. In Fig. 2 we show results for the eyeball saccade profile $x(t)$ calculated with Eq. (4) for different values of the parameters. First, in Fig. 2(a) we consider various values of x_m at fixed A, μ, and β. Thus,

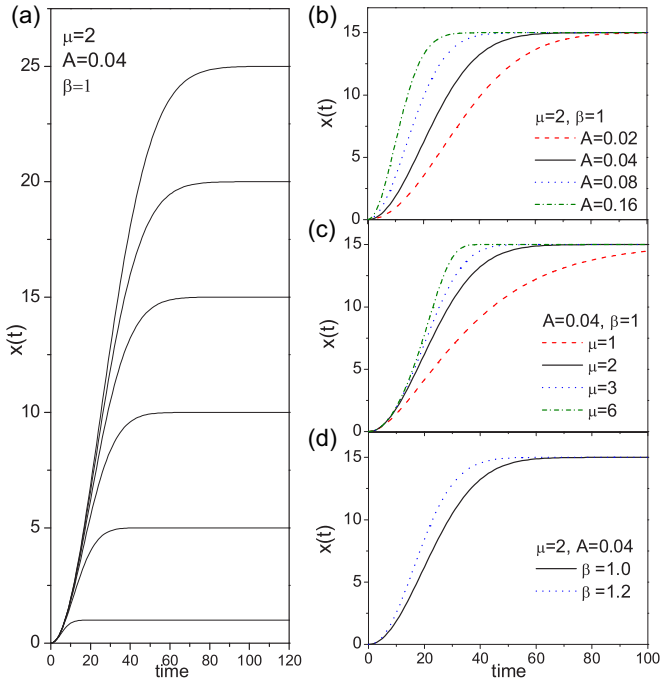

FIG. 2. Eyeball dynamics. (a) Eyeball position $x(t)$ for a family of saccades with fixed $\mu = 2$, $\beta = 1$, $A = 0.04$ and various values of x_m. These saccades satisfy the relation given in Eq. (7). Panels (b), (c), and (d) show $x(t)$ calculated for $x_m = 15$ considering different values of A, μ, and β, respectively.

the set shown corresponds to what we have previously called a family of saccades within the constant parameter approximation, and models a set of saccades that would be obtained from a single eye in a fixed direction. Importantly, these saccades satisfy $\mathrm{Max}[\dot{x}] \propto x_m^{1/2}$, according to Eq. (7) with $\mu = 2$ and $\beta = 1$. Then, Figs. 2(b), 2(c) and 2(d) consider a fixed saccade size $x_m = 15^\circ$ and analyze the dependence on A, μ, and β, respectively. In Fig. 2(b) we see that the saccade time (i.e., the time required to get to the saccade size) decreases with the parameter A. Moreover, the initial acceleration (that for $\beta = 1$ coincides with A) trivially grows with A. In Fig. 2(c) we see that when μ grows at constant A and β the saccade time also decreases, but the initial accelerations remains constant. In this case, it is equal to A but it would be equal to zero for $\beta > 1$. Finally, Fig. 2(d) shows that the saccade time also decreases with growing β.

It is worth noting that the dynamics of $x(t)$ is always monotonic. Neither oscillations nor eyeball overshooting occurs for any value of the parameters.

VI. PUPIL DYNAMICS FOR THE MODEL WITH CONSTANT PARAMETERS

Here we present the results for the pupil dynamics calculated with constant k and γ, and we analyze the influence of each parameter. To calculate the pupil position $x(t) + y(t)$ we use the formulas in Eqs. (4) and (15) and check them with a standard high-precision numerical integrator [9]. The analytical solutions result indistinguishable from the numerical ones when considering a large enough number of terms in the expansion of $y(t)$. For practical purposes, between 20 and 400 terms are usually enough, depending on the parameters. Further details on the convergence properties of the analytical solutions are given in the Appendix.

To get a first insight about the role of each parameter it is worth analyzing the physical mechanisms involved in a saccade according to the model. The curves in Figs. 1(a) and 1(b) indicate that, at the beginning of the saccade the pupil starts to move later than the eyeball, while at the end of the saccade, when the eyeball decelerates, the pupil overcomes it. This is due to the combined effect of the inertia and the elastic force. Loosely speaking, at the beginning we have $y(t) \sim 0$ and thus the elastic force $-ky(t)$ is small, so that the pupil motion is delayed. At the middle of the saccade, when the elastic force is large enough, the eyeball and pupil move at similar velocities (the pupil is actually slightly faster). Finally, at the end of the saccade, the eyeball decelerates while the pupil keeps on moving fast due to its inertia, until it is stopped and dragged back by the elastic force and it begins to perform a damped oscillation. The whole process, that was nicely described in Ref. [18], is similar to what a person experiments inside a car when the car accelerates and brakes. The PSO shape is determined by the competition between the inertial and elastic forces. Regarding the role of the parameters in this competition, it is worth noting that, while k controls the stiffness of the elastic force, a growth of any of the parameters A, μ, and β enhances the accelerations (and decelerations) and thus leads to stronger inertial forces. The parameter γ controls the way in which the relative motion is damped. In particular, it regulates the damping of the PSO. It is important to mention that, as far as we know, there is still no experimental evidence of the existence of an initial delay of the pupil with respect to the eyeball. Later we discuss on possible modifications of the model if such an effect was definitively ruled out by future experiments.

A. Influence of the parameters on the families of saccades

In Fig. 3 we analyze the dependence on the parameters of the profiles for families of saccades generated with constant A, μ, β, k, and γ. First, Fig. 3(a) shows the effect of varying the parameter μ. We see that the amplitude of the PSO grows with μ, especially at large x_m. This can be understood by noting that, as Fig. 2(c) shows, a larger value of μ produces a faster saccadic motion and consequently a more sudden deceleration. In addition, we see that the time for the first overshoot decreases with μ, as expected. The effect of changing the parameter μ is relatively smooth at small times. In particular, the initial acceleration remains invariant, as previously mentioned.

The family of saccades for $\mu = 2$, $A = 0.06$, $k = 0.032$, $\gamma = 0.15$, shown in black dotted lines in Figs. 3(b), 3(c) and 3(d) is now taken as a reference to analyze the influence of the parameters. Figure 3(b) shows the effect of changing A at fixed μ, β, γ, and k. We see that the PSO amplitude grows with A for all x_m, clearly this is for the same reason as it does with μ. However, a change in A affects not only the end of the saccade and the main ascending slope, but also the beginning of the saccade.

In Fig. 3(c) we show the effect of varying the parameter k, i.e., the stiffness of the effective elastic link between the pupil

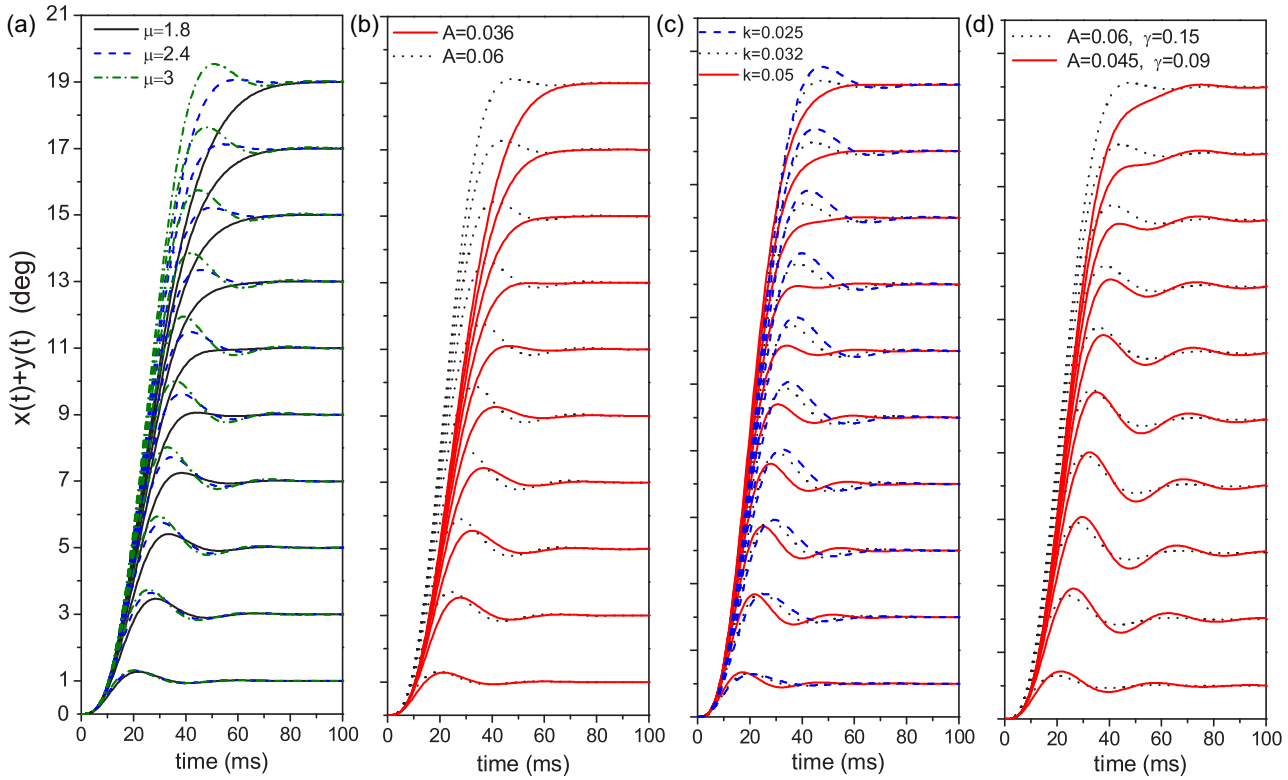

FIG. 3. Dependence of the pupil motion on the model parameters. (a) The curves show how the value of μ influences the saccade profiles for a family obtained with constant A, μ, β, k, and γ. (b) Dependence on A of the saccade profiles from a family. (c) Dependence on k. (d) Variations with A and γ. In panels (b), (c), and (d), the family of saccades plotted in dotted lines is the same as the one in Fig. 1(a).

and the eyeball. The amplitude of the PSO is found to decrease with k, as could be expected. Moreover, a change on this parameter affects mainly the end of the saccade. The effect of increasing k is in fact similar to that of decreasing μ, although for different (but perhaps complementary) reasons. While a decrease in μ leads to a reduction of the inertial effects at the end of the saccade, an enhancement of k increases the elastic force which opposes to the inertial force.

Finally, in Fig. 3(d) we show the effect of a combined change of A and γ. We see that the model is able to produce saccadic profiles with the first overshoot below the level x_m, resembling qualitatively some experimental saccades which share this property [15] (below we further discuss this issue). The effect of decreasing γ (i.e., the damping), which corresponds to an enhancement of the PSO amplitudes and *lifetimes*, is apparent for small x_m saccades. For large values of x_m it is hidden by the effect of reducing A.

Although the results in Fig. 3 do not attempt to fit particular experiments but just to analyze the dynamical properties of the model and the dependence on the parameters, it is worth observing the qualitative similarity between the generated curves and the experimental saccades found in Ref. [15] and other works. Moreover, when varying the parameters as in Fig. 3, the solutions exhibit qualitative changes similar to those found in experimental families in Ref. [15] when the direction of the saccade is varied. For instance, in Ref. [15], the comparison between upward and downward vertical saccades for the same observer shows that, for each saccade size, upward saccades have larger PSO amplitude than downward saccades in four observers over five (Fig. 9 in Ref. [15]). Moreover, although more data is needed for a confirmation, larger PSO amplitudes seem to be correlated with larger peak velocities (Fig. 8 in Ref. [15]). Within our model it is possible to enhance the PSO amplitude together with the peak velocity by increasing the parameter A, as shown in Fig. 3(b). This suggest that, for a given eye, upward saccades should be modeled using a larger value of A than the one used for downward saccades. Certainly, an accurate fitting may require, in addition, to change the parameter μ (or β as well), which also modulate the PSO amplitude, although with smaller modifications on the saccade velocities. These results lead us to interpret that the muscles exert a larger force when moving upward than when moving downward. Note that, although a change in the parameter k may also lead to similar variations on the PSO amplitudes, as a first approach, we do not expect that the effective viscoelastic properties of the eye (characterized by k and γ) should vary with the direction.

The comparison of experimental horizontal saccades for adduction and abduction (see Fig. 2 in Ref. [15]) leads to similar but less clear conclusions. For three of the four eyes studied in [15], the PSO amplitude is larger for abduction than for adduction, although the differences are not as large as in the comparison between upward and downward saccades. Moreover, for the other eye (Obs 2 right eye in Fig. 2 in Ref. [15]) there is no appreciable difference between adduction and abduction. This all also suggest a possible decrease in A or μ when changing from abduction to adduction, but this may depend strongly on the observer and more cases

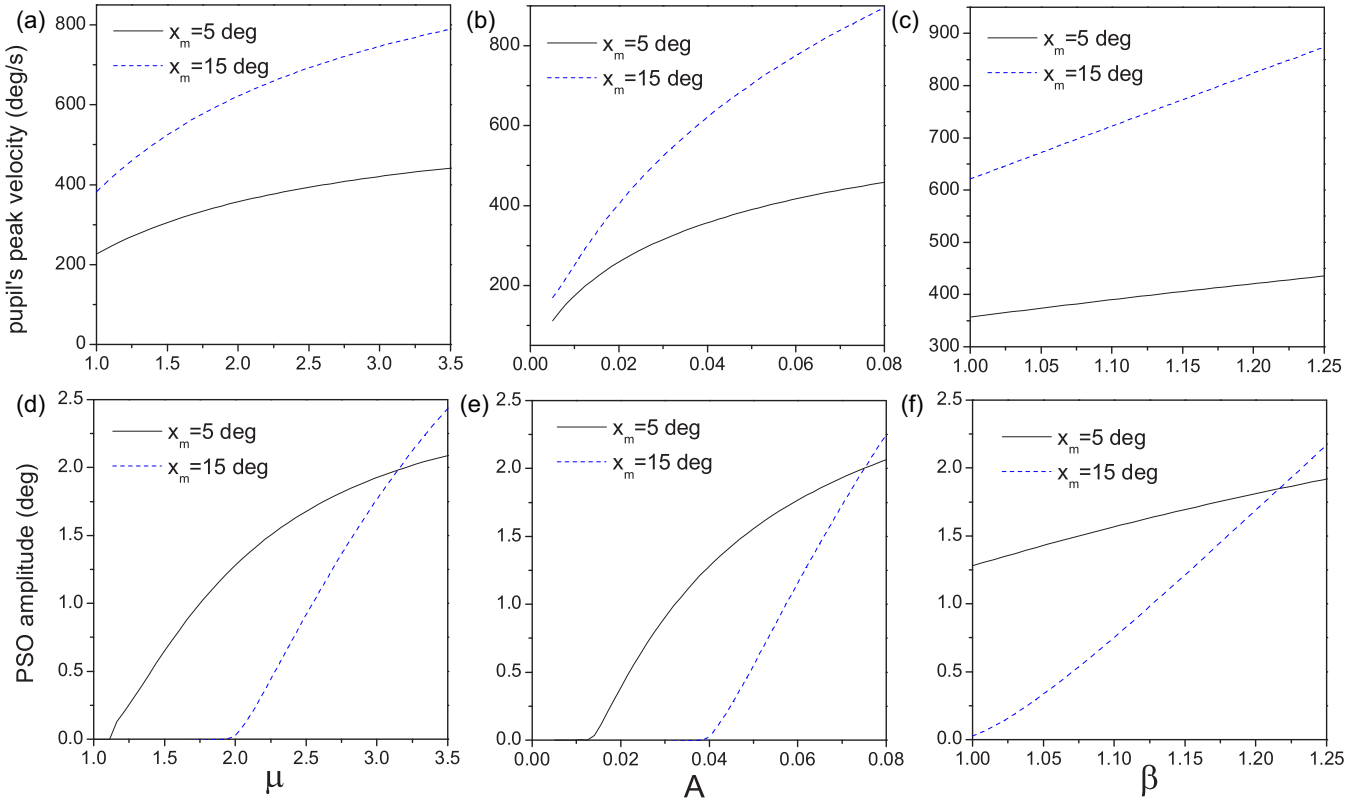

FIG. 4. Dependence of the peak velocity and the PSO amplitude on the parameters of the eyeball dynamics. Panels (a), (b), and (c) show the dependence of the pupil's peak velocity on the parameters μ, A and β, respectively, considering the indicated values of saccade size. Panels (d), (e), and (f) show the corresponding behavior of the PSO amplitude. In all the cases the curves correspond to $k = 0.03$ and $\gamma = 0.1$, while the eyeball parameters are $A = 0.04$, $\mu = 2$, and $\beta = 1$ except when each parameter varies.

should be analyzed to get clear conclusions. In any case, we here observe that the different directions of motion should in general be characterized by different values of A and μ.

In addition, experiments show that the amplitudes of the PSO for the same task vary between individuals [15], with relevant effects of aging [19]. This could be due to variations both in the parameters characterizing the forcing profiles (μ, A, and β) and in those associated to the viscoelastic properties (k and γ).

B. Analysis at fixed saccade size: The onset of PSO

Now we focus on the dependence of the peak velocity and the PSO amplitude on the system parameters at fixed saccade size. For this, we consider two saccade sizes, namely, $x_m = 5^\circ$ and $x_m = 15^\circ$, and then vary the rest of the parameters around reference values given by $A = 0.04$, $\mu = 2$, $\beta = 1$, $k = 0.03$, $\gamma = 0.1$. It should be remarked that the PSO amplitude here considered is the one associated to the first overshoot, as defined in Fig. 1(e).

In Fig. 4 we analyze the role of the eyeball parameters A, μ, and β. Figures 4(a), 4(b), and 4(c) show that, as anticipated, the peak velocity grows with these parameters. Moreover, the growth is faster for $x_m = 15^\circ$ than for $x_m = 5^\circ$. However, Figs. 4(d), 4(e), and 4(f) show that the PSO amplitude increases with A, μ, and β as previously indicated, due to the enhancement of the inertial effects mentioned before. Two features are remarkable. First, at low values of A or μ, the PSO amplitude is zero, while it becomes non zero in a critical-like fashion at certain values of the parameters. The critical values are larger for $x_m = 15^\circ$ than for $x_m = 5^\circ$. Hence, there are regions of the parameters for which the PSO are nonzero for $x_m = 5^\circ$ and zero for $x_m = 15^\circ$, in agreement with that shown when analyzing the families of saccades. Second, at large values of A, μ, or β, the PSO amplitude for $x_m = 5^\circ$ is smaller than that for $x_m = 15^\circ$. This contrast the observations of most of the experiments in Ref. [15] so that such regions of parameters could be considered physically irrelevant. For instance, $\mu > 3$, $A > 0.7$, or $\beta > 1.2$ for the parameters considered. However, it should be noted that experiments in Ref. [19] (and also Ref. [15]) show exceptional behaviors for a few particular observers for which the PSO amplitude seems to grow at large x_m. This deserves further research.

In Fig. 5 we analyze the dependence of the peak velocity and the PSO on the parameters k and γ. The peak velocity is found to depend smoothly on these parameters confirming that it is essentially determined by the movement of the eyeball. In contrast, as expected, the PSO amplitude depends strongly on k and γ. In the relevant regions, the PSO amplitude decreases with k and γ and becomes zero at a critical value that depends on x_m. For very low k, the PSO amplitude for $x_m = 15^\circ$ equals that for $x_m = 5^\circ$ implying that such a region of parameters would be of no relevance for most observers.

In Fig. 6 we analyze how the PSO profiles change when a parameter passes through a critical value. First, we focus on

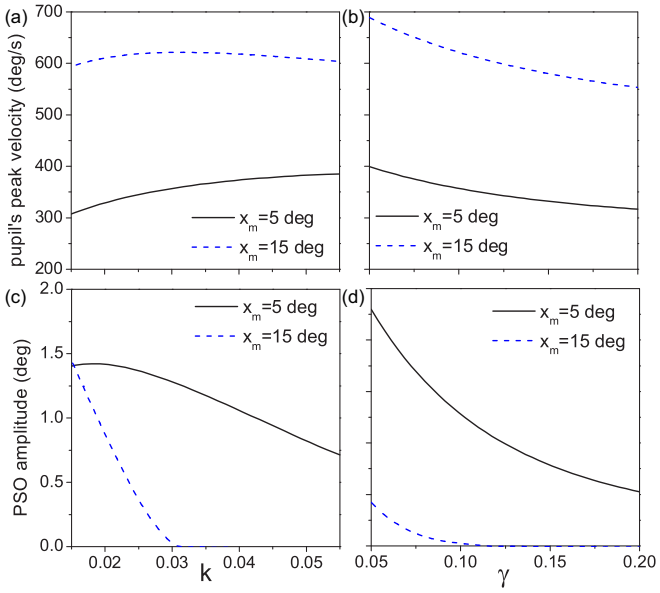

FIG. 5. Dependence of the peak velocity and the PSO amplitude on k and γ. Panels (a) and (b) show the dependence of the pupil's peak velocity on the parameters k and γ, respectively, considering the indicated values of saccade size. Panels (c) and (d) show the corresponding behavior of the PSO amplitude. In all the cases the eyeball parameters are $A = 0.04$, $\mu = 2$, and $\beta = 1$, while we considered $k = 0.03$ and $\gamma = 0.1$ except when indicated.

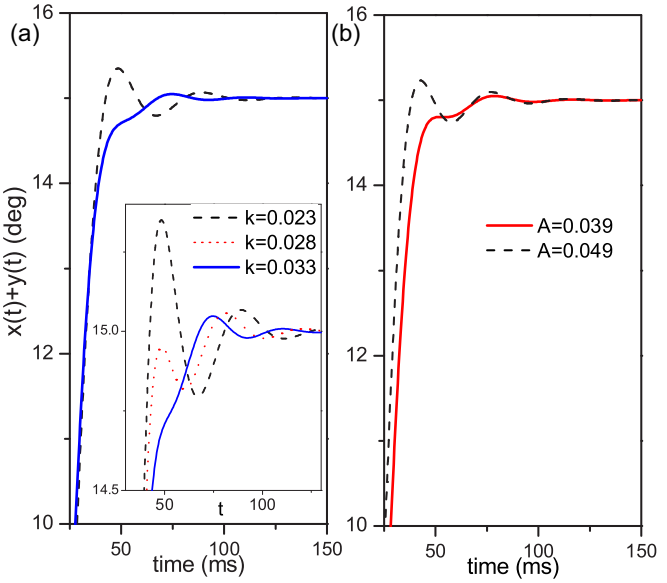

FIG. 6. Dependence of the saccade profiles on the parameters around the critical values (a) Saccades for $k = 0.023$ ($<k_c$) (black dashed line) and $k = 0.033$ ($>k_c$) (blue solid line) corresponding to the set with $x_m = 15°$ analyzed in Fig. 5(c). The inset shows details of the same curves in a different scale and an additional profile for $k = 0.028$ (dotted red line). (b) Saccades for $A = 0.049$ ($>A_c$) (black dashed line) and $A = 0.039$ ($\simeq A_c$) (red solid line), both corresponding to the set with $x_m = 15°$ analyzed in Fig. 4(e).

what happens with the parameter k. We consider the example illustrated in Fig. 5(c), for which the critical value is $k_c \simeq 0.03$. In the main panel of Fig. 6(a) we show two saccade profiles. The dashed curve corresponds to $k = 0.023$ (i.e., $k < k_c$), while the solid one is for $k = 0.033 > k_c$. We see that the first overshoot disappears for $k > k_c$ [this is why the PSO amplitude vanishes according to our definition sketched in Fig. 1(e)]; however, the second overshoot is still observable. In the inset in Fig. 6(a) we show the detail of the PSO profiles for the same two saccades and we also include a third profile corresponding to an intermediate value of k. It is apparent that, when k grows, the amplitude of the first overshot decreases until it disappears, while the second peak moves to the left. In Fig. 6(b) we show that a similar transition occurs when the parameter A crosses the critical value, although in this case the second overshoot remains fixed. According to our results in Fig. 3(d), the same type of transition is found by increasing x_m, for some parameter sets. Other calculations (not shown) confirm that the same occurs when decreasing the value of μ below the critical value. Hence, the mechanism for emergence (or vanishing) of the PSO when the parameters are varied seems rather general. Importantly, as mentioned before, the PSO profiles in which the first overshoot is rubbed out while the second survives [like those shown in Figs. 3(d) and 6] are frequently observed in experiments. For instance, see Ref. [15]. Moreover, just before the complete vanishing of the first overshoot, there is a small region in which the first peak of the PSO is below the asymptotic level x_m and of smaller amplitude than the second peak [inset of Fig. 6(a), red dotted curve]. These types of profiles are also observed in the experiments of Ref. [15].

VII. FITTING FAMILIES OF SACCADES: BEYOND THE CONSTANT PARAMETERS ASSUMPTION

The model with constant parameters allows to describe most of the phenomenology of the saccadic and PSO's dynamics, including the qualitative dependence of the PSO profiles on x_m. In this way, it provides a simple explanation for the emergence of the PSO in terms of elastic and inertial forces. However, as discussed in Ref. [9], an accurate fitting of a family of averaged saccades (or a set of families from different individuals) may require more complex formulations. It has to be noted that the model is an effective description that cannot encompass all the details of the PSO dynamics, probably involving complex viscoelastic processes, three dimensional deformations and strong variations among individuals.

In Ref. [9] an example of fitting of a particular family of saccades taken from experiments was provided by considering a *force-dependent* parameters model. Such a formulation assumes that the parameters k and γ depend on the forcing $F(t)$ as $\gamma[F(t)] = \gamma_0 \exp[-cF(t)]$ and $k[F(t)] = k_0 \exp[-dF(t)]$, with $c, d > 0$. This represents a loosening of the eyeball-iris link with the force, which enables larger PSO amplitudes at large x_m. The idea beyond the approximation is that the forces exerted on the eyeball may not only rotate it but also produce smooth deformations which can change the viscoelastic properties. Within this model, a family of saccades is generated by keeping A, μ, β, k_0, γ_0, c, and d constant, and varying only the saccade size x_m. The family presented in Ref. [9], that fits accurately averaged saccades from a single observer in Ref. [15], is reproduced in Fig. 7(a). Then, in Figs. 7(b), 7(c) and 7(d) is reproduced again in gray lines in order to compare with other models.

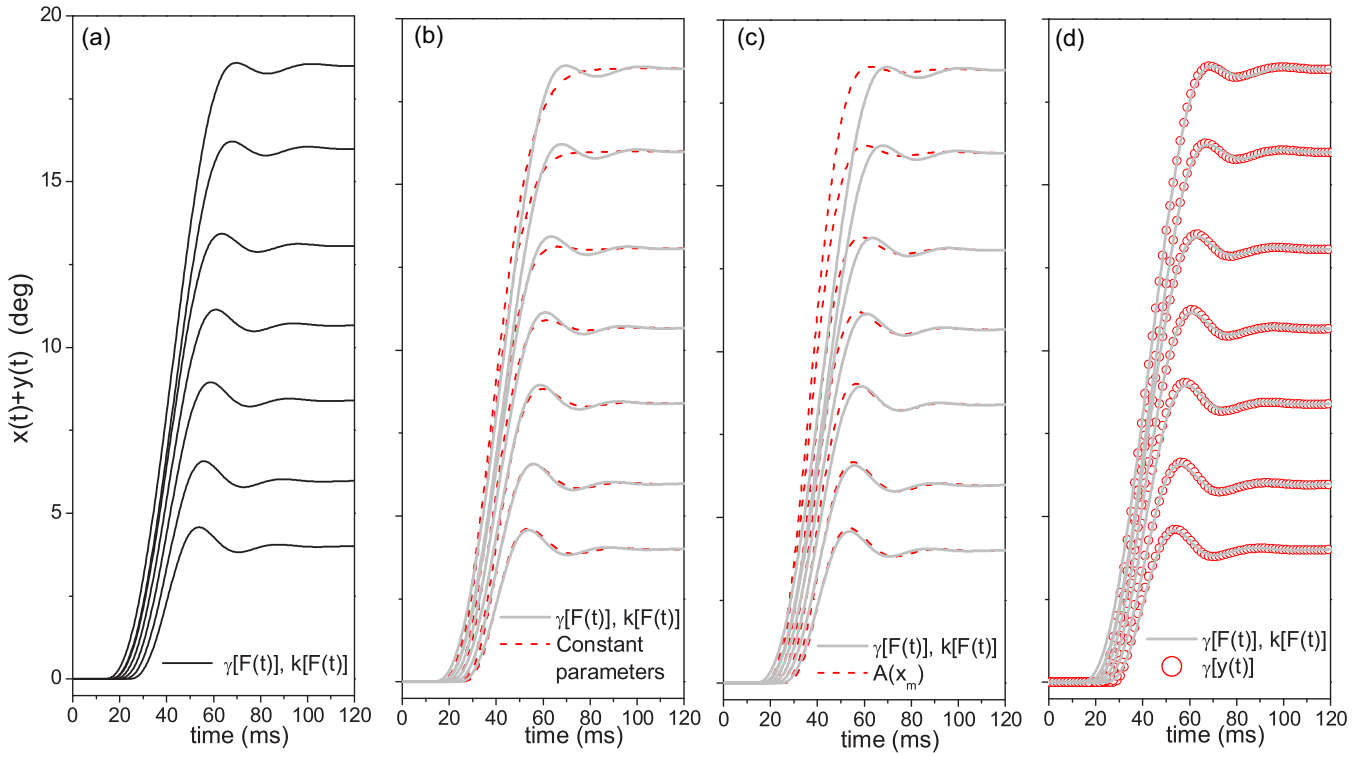

FIG. 7. Families of saccades beyond the constant parameter approach. (a) Family of saccades calculated with the model with force dependent parameters for $A = 0.036$, $k_0 = 0.04$, $\gamma_0 = 0.14$, $c = 0.5$, and $d = 3$ that was shown in Ref. [9] to match a particular experimental family taken from Ref. [15]. This calculated family is repeated in panels (b–d) in gray lines. (b) The red dashed curves correspond to a family calculated with constant parameters $A = 0.04$, $k = 0.032$, $\gamma = 0.15$. (c) The red dashed curves correspond to a model with constant parameters for each saccade, but with A dependent on x_m, considering $A = 0.36 + 0.0012x_m$, and fixed $k = 0.032$, $\gamma = 0.14$. (d) The red circles show a family computed with the inhomogeneous viscosity model considering $A = 0.05$, $k = 0.035$, $g_0 = 0.07$, $a = 1$, $b = 5$. All the calculations are for $\mu = 2$, $\beta = 1$.

The model with force dependent parameters was proposed because the constant parameter version produces a decay of the PSO amplitude with x_m faster than that observed in the experiments. This is shown in Fig. 7(b), where we depict a family of saccades generated with constant parameters at fixed A, μ, β, k, and γ and varying x_m. The results correctly fits the $x_m = 4^\circ$ of the experimental family, while fail at fitting the saccades with large x_m. Note that, for simplicity, we compare with the force-dependent model (that approximates the experiments for all x_m [9]) instead of with the experiments themselves.

The assumption of force-dependent parameters is certainly a reasonable one to moderate the decay of the PSO amplitude with x_m, but it is not the only possible one. Here we propose and discuss other two formulations that may also be sound. First, we note that, to generate a family of saccades, we can keep on using the dynamics with constant parameters for each saccade, but considering that one or more parameters depend on x_m. The results in the previous section indicate that the PSO amplitude grows with A, μ, and β. Thus, one possibility is to consider that one or more of these parameters grows smoothly with x_m. This could be reasonable since the muscles that rotate the eyeball may act in different ways for each saccade size. Note that, in contrast, a dependence of the parameters k or γ on x_m would be meaningless. As an example, in Fig. 7(c) we show a family of saccades generated with the model with constant parameters assuming that A grows with x_m as $A = 0.36 + 0.0012x_m$, while μ, β, γ, and k are kept fixed. The dependence of A on x_m was chosen in such a way that the PSO amplitude matches that from the experiments for every x_m. The approach, however, fails at predicting the saccade velocities, which at large x_m results larger than the experimental ones. This could be expected, since a change on A with x_m affects the relation between the peak velocity and x_m. The effect is shown in Fig. 8 where we plot the peak velocity as a function of x_m for the various models considered in Fig. 7. The fact that, for our example, the model with $A = A(x_m)$ overestimates the peak velocity at large x_m is apparent. However, we have to take into account that this is just the analysis of a family of saccades arbitrarily chosen from a particular individual. In general, the consideration of a smooth dependence of the parameters A, μ, or β on x_m may not necessary affect considerably the behavior of the peak velocity (depending on the whole set of the parameters) and could be of relevance. A final answer to this feature should come from experiments that measure the peak velocity of the eyeball (not the pupil) as a function of the saccade size. In case that such experiments found a *pure* power law with a single exponent, the parameters should be kept independent of x_m. In contrast, if the exponent depends on x_m, non constant values of A, μ, or β may be relevant.

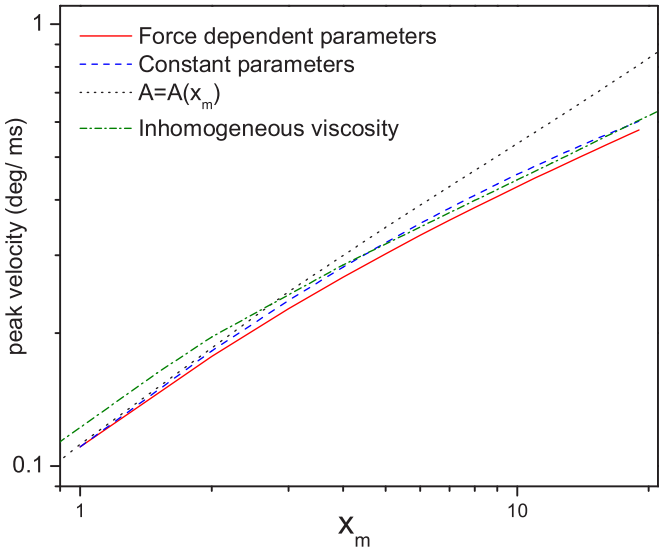

FIG. 8. Peak velocity beyond the constant parameter approach. Pupil's peak velocity as a function of the saccade size calculated for the models and parameters indicated in the caption of Fig. 7.

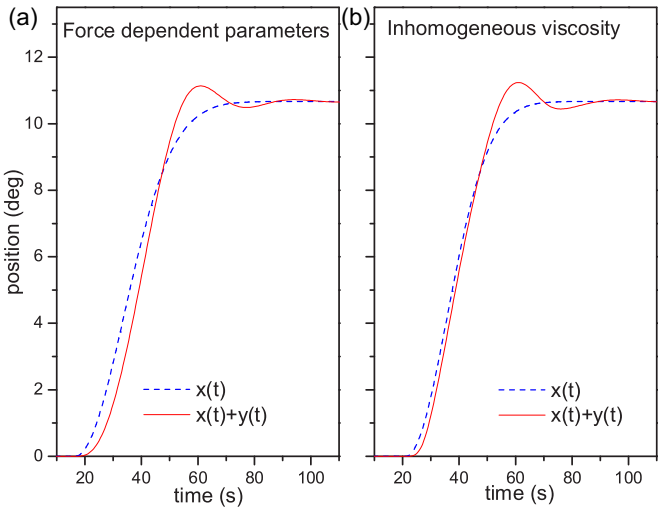

FIG. 9. Force dependent vs. space dependent parameters. (a) Detail of the 10° saccade for the model with force dependent parameters shown in Figs. 7(a)–7(d) exhibiting pupil and eyeball motion. (b) Detail of the 10° saccade shown in Fig. 7(d) for the model with inhomogeneous viscosity.

Finally, we consider a model in which the viscosity γ depends on the position of the pupil along the direction of the saccade. We assume the simple form $\gamma = \gamma[y(t)] = \gamma_0\{1 + a\exp[-by(t)]\}$. Note that this represents a decay of the viscosity with the distance to the equilibrium position $y = 0$ measured along the direction of the saccade ($y > 0$), and an enhancement of the viscosity in the opposite direction ($y < 0$). This means that the inhomogeneity is *activated* when the saccade starts. As in the *force dependent* model, here we are also assuming that, during the saccade, the eyeball suffer deformations that change the viscoelastic properties. For simplicity the approach is referred to as model with *inhomogeneous viscosity*. In Fig. 7(d) we show a family of saccades generated with this model at fixed A, μ, β, k, γ_0, a, and b that results almost coincident with the family generated with the *force dependent* model. As can be seen in Fig. 8, excepting for low values of x_m, the peak velocity of the two models are very similar. Still, there is a subtle detail that differences the two generated families of saccades. As shown in Fig. 9, the time delay between the motion of the eyeball and that of the pupil is much larger for the force dependent model than for the model with inhomogeneous viscosity. Note that such a delay is associated to a larger displacement $|y(t)|$ of the pupil with respect to the eyeball at small times. As mentioned, there is no experimental evidence of such a delay, that is a natural prediction of the model. In the case that the delay was ruled out by experiments, the effect in the model dynamics could be moderated by introducing an inhomogeneous viscosity (as shown) or possible by introducing a static friction force acting at the beginning of the saccade.

The particular example studied in Figs. 7, 8, and 9 serves to show how the different versions of the models could work in extensive analyses of experiments. It is important to indicate, however, that the experiment here analyzed correspond to p-Cr signals [15,16], so that the curves may not reflect exactly the pupil motion [16], and thus the fitted parameters k and γ may not correspond to the effective elasticity and viscosity for the relative motion of the pupil. According to the preliminary studies in Ref. [9], to recover the original meaning of these parameters, the P-Cr signal should be fitted by $x(t) + \lambda y(t)$, with $\lambda \sim 2$ but possible dependent on x_m and on the eye tracking technique. Although this subject requires further research (and ideally a separate modeling of the dynamics of the corneal reflection), the parameter λ could be considered as an additional variable to fit when attempting to reproduce P-Cr signals. Note that throughout this paper we have considered $\lambda = 1$.

VIII. SUMMARY, FINAL COMMENTS, AND CONCLUSIONS

In this paper we have provided analytical solutions for the model for eyeball and pupil motion developed in Ref. [9] and studied its dynamical properties, as well as the role of the system parameters. Moreover, we have discussed various alternative versions of the model and generalizations that may serve to obtain better descriptions of the experiments, and to perform a step forward in the understanding of saccadic motion and PSO. Our approach enables an analysis of the saccadic motion in the time domain, which is relevant to gain insight concerning the results from experiments such as those in Refs. [15,16]. However, it is important to mention that, within the fields of bioengineering and neuroscience, the eye motion is usually analyzed in the frequency domain since it is more natural from the view point of many experiments [24,28,29].

The model developed has two key ingredients. On the one hand, the particular function $F(t)$ defined in Eq. (3) that approximates the velocity of the eyeball along the saccade. On the other hand, the consideration of the pupil as a massive particle subject to the competition between inertial forces produced by the eyeball rotation and viscoelastic forces inside the eyeball. Altogether, these assumptions provide a unified description for the findings of independent experiments concerning (i) the peak velocity as a function of the saccade size

x_m and (ii) the PSO amplitude and period as functions of x_m. To obtain the qualitative behaviors found in experiments it is enough to consider the *constant parameter* version of the model, in which μ, β, A, k, and γ are constant and independent of the saccade size x_m, while only the parameter τ in Eq. (3) is adapted to get the desired value of x_m, according to Eq. (6). In this approach, the parameters μ, A, and β could be varied to reproduce saccades on different directions for the same eye. Meanwhile, the parameters k and γ could be kept invariant for the different directions, but should change among observers.

The search for accurate fittings of families of saccades from particular observers would require to go beyond the constant parameter approach. For instance, we may consider parameters that depend on x_m (but still constant for each saccade), or include a dynamical dependence of some parameters on $F(t)$ or on the relative position of the pupil. Even more, we may think on proposing a different function $F(t)$, taking care that the alternative should ensure a suitable relation between the peak velocity and the saccade size. However, the most important deviations from the constant parameter approach seem to occur for relatively large values of the saccade size, for which the decreasing of the PSO amplitude with x_m observed seems to be sensibly slower than the prediction of the model [9]. The constant parameter approach may thus be a reasonably option at relatively small saccade sizes, such as $x_m < 10^\circ$. Nevertheless, it should be remarked that the PSO amplitude depends on the eye tracking technique and, nowadays, the experimental data concerning the characterization of the PSO is limited, noisy and show strong variations among individuals. More experimental efforts, particularly concerning statistics on the PSO behavior for different saccade sizes and directions would be needed in order to be able to refine a model. Ideally, it would be desirable to perform experiments such as those in Ref. [15], where the observers are asked to make saccades between the two dots separated either horizontally or vertically, but varying both the initial and final position of the dots systematically throughout the screen and with many observers. In this way we could perform statistics on saccades of different sizes, directions and also varying the initial position with respect to the center.

Within our model, the action of the nervous system is included through the function $F(t)$, which describes the activity (governed by neural signals) of the muscles that rotate the eyeball during a single saccade. The profiles proposed for $F(t)$ are such that the motion of the eyeball within an individual saccade is unidirectional, with no oscillations and no feedback mechanism. This assumption is enough to obtain all the results shown concerning PSO. Hence, our developments strongly suggest that PSO are mainly consequences of mechanical reactions inside the eyeball prompted by inertial and viscoelastic forces. This agrees with recent suggestions from experimentalists [16] and with the fact that eye wobbling is a well established phenomenon. According to our vision, feedback mechanisms and oscillations of the eyeball governed by the nervous system may be negligible within single saccades and PSO, although they are essential for ruling successions of saccades and other types of eye motion such as smooth pursuit.

In this paper we extended the original proposal for $F(t)$ by including the parameter β, which has an interesting role. The initial acceleration of the eyeball vanishes for $\beta > 1$ while it is given by the parameter A for $\beta = 1$. Hence, the determination of the initial acceleration of the eyeball would directly provide an estimation for β and possible for A. However, such a determination may not be straightforward since it perhaps should involve an analysis of the position of the pupil (the usual output of the eye trackers). For this, one may consider small time expansions of the analytical solutions of the model.

The analytical solutions presented may be useful for studying limit cases and performing expansions not only at small times, but also at large times or, for instance, around the time of maximal velocity. Moreover, it is possible to think of performing series expansions in terms of the parameters around values of particular relevance. Such types of studies, which are beyond the scope of this paper, could contribute to find additional relations between parameters and dynamical properties, and to develop easier ways for fitting the parameters to experimental data.

The analysis in Figs. 4 and 5 reveals that the PSO emerge (or are suppressed) in critical-like ways when some of the parameters variate. The proximity to criticality is characterized by PSO profiles in which the amplitude of the first overshoot is smaller than that of the second. This type of patterns are usually observed in eye tracking signals. Detailed studies of these phenomena are desirable from a theoretical point of view and could enrich the understanding of the PSO behavior. The analytical solutions may be useful for identifying the critical values of the parameters and studying the PSO onset.

Very generally, the fact that the model correctly reproduces the different type of PSO patterns observed in experiments as well as the dependence on x_m of the PSO amplitude and period (and the peak velocity as well) strongly suggests that the basic mechanism ruling the PSO is the one considered in the model. This means the competition between inertial and viscoelastic forces within the eyeball.

Experiments show that the PSO's characteristics vary among observers [15] and change with aging [19]. Moreover, PSO may be suppressed in patients with cataract surgery [19]. These facts indicate that the PSO dynamics is likely related to anatomical or physiological conditions of the eye, that may be eventually affected by diseases. Our model can certainly be used as a simple but powerful tool for interpreting experiments concerning these relevant features.

ACKNOWLEDGMENTS

The authors acknowledge support from CONICET through the PIP program, and from CNEA, both Argentinian agencies. We also acknowledge funding from Universidad Nacional del Sur, through PGI 24/F065. We thank Marcos M. Meo for a careful reading of the manuscript.

APPENDIX

In this Appendix we give the definitions of the special functions used in the main text and we explain the convergence properties of the analytical solutions provided.

1. Definitions of the special functions used in the analytical solutions

The Kummer [25,26] function is a confluent hypergemetric function [25,26]. One of its multiple definitions is

$$ {}_1F_1(a,b;z) = \sum_n \frac{(a)_n}{(b)_n}\frac{z^n}{n!}, \tag{A1}$$

where the Pochhammer symbol [26] $(\gamma)_n = \Gamma(\gamma+n)/\Gamma(\gamma)$ is defined in terms of the Γ function [25],

$$ \Gamma(z) = \int_0^\infty t^{z-1}\, e^{-t}\, dt. \tag{A2}$$

The power series of Eq. (A1) converges absolutely for all value of the variable z.

The exponential integral function $Ei(\nu, z)$ is an analytical function of ν and z which is defined in whole complex plane of both variables. This function can be expressed in terms of the Kummer function as follows [26]:

$$ Ei(\nu,z) = \Gamma(1-\nu)z^{\nu-1} - \frac{1}{1-\nu}\,{}_1F_1(1-\nu, 2-\nu, -z). \tag{A3}$$

2. Convergence of the analytical solutions

As indicated in the main text, the analytical solutions are indistinguishable from the numerical ones when we consider a large enough number N of terms in the expansion of $y(t)$ given in Eq. (16) or Eq. (17) (the latter only for $\mu = 2$). In Fig. 10 we show how the analytical solution converges to the numerical one as N grows. It can be seen that a very small N is enough for reproducing the solution at small times (in this particular example, even $N = 1$ is suitable for $t < 20$ ms), while an increasing number of terms is needed at large times. Note that expansions with an even number of terms tend to $+\infty$ at large times, while expansion with odd N diverge to negative values. Our analysis of various cases indicate that the convergence at large t becomes slower (i.e., more terms are needed) for relatively small values of x_m, large values of μ or A, or small values of k.

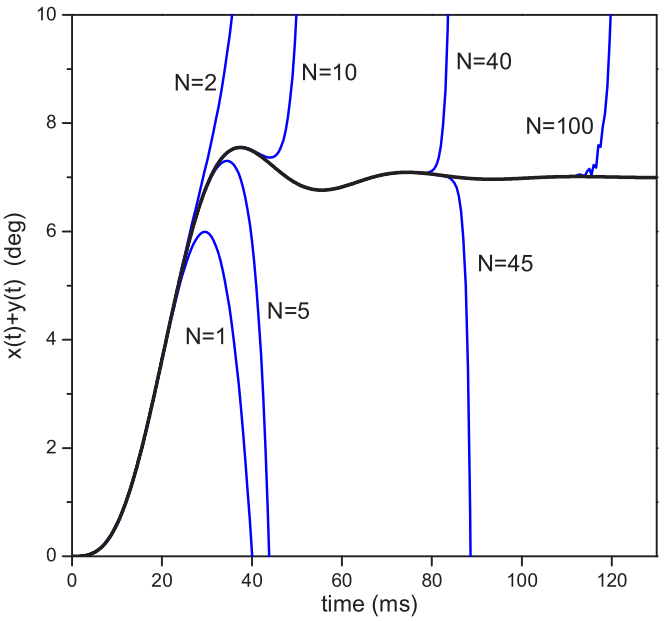

FIG. 10. Convergence of the analytical solution. The solid black curve shows the numerical solution for $x(t) + y(t)$ for a saccade generated with the model with parameters $A = 0.03$, $\mu = 2.1$, $\beta = 1$, $\gamma = 0.1$, $k = 0.03$, and $x_m = 7$. The blue lines show the analytical results calculated from Eqs. (4) and (16) considering an increasing number (N) of terms for approximating the expansion in Eq. (16). For this particular set of parameters, the solution for $N = 150$ (not shown) is indistinguishable from the numerical one in the scale of the plot up to $t = 130$.

[1] A. L. Yarbus, *Eye Movements and Vision* (Plenum Press, New York, 1967).

[2] H. Collewijn, C. J. Erkelens, and R. M. Steinman. J. Physiol. **404**, 157 (1988).

[3] A. Duchowski, *Eye Tracking Methodology*, 3rd ed. (Springer, Berlin, 2017).

[4] G. Boccignone and M. Ferraro, Physica A **331**, 207 (2004).

[5] D. Shinde, A. Mehta, and R. K. Mishra, Europhys. Lett. **94**, 68001 (2011).

[6] J. I. Specht, L. Dimieri, E. Urdapilleta, and G. Gasaneo, Eur. Phys. J. B **90**, 25 (2017).

[7] T. A. Amor, S. D. S. Reis, D. Campos, H. J. Herrmann, and J. S. Andrade, Jr., Sci. Rep. **6**, 20815 (2016).

[8] J. Tabernero and P. Artal, PLoS ONE **9**, e95764 (2014).

[9] S. Bouzat, M. L. Freije, A. L. Frapiccini, and G. Gasaneo, Phys. Rev. Lett. **120**, 178101 (2018).

[10] W. J. Yuan, J. F. Zhou, and C. Zhou, Phys. Rev. E **93**, 042302 (2016).

[11] J. F. Zhou, W. J. Yuan, and Z. Zhou, Sci. Rep. **6**, 35255 (2016).

[12] J.-R. Liang, S. Moshel, A. Z. Zivotofsky, A. Caspi, R. Engbert, R. Kliegl, and S. Havlin, Phys. Rev. E **71**, 031909 (2005)

[13] K. Mergenthaler and R. Engbert, Phys. Rev. Lett. **98**, 138104 (2007)

[14] M. Nyström, I. Hooge, and K. Holmqvist, Vision Res. **92**, 59 (2013).

[15] I. Hooge, M. Nyström, T. Cornelissen, and K. Holmqvist, Vision Res. **112**, 55 (2015).

[16] I. Hooge, K. Holmqvist, and M. Nyström, Vision Res. **128**, 6 (2016).

[17] The reader may find on the internet several interesting videos on the subject.

[18] K. Wright, *Focus: Why Your Pupils Wobble*, Story about Ref. [9], Phys. Rev. Lett., Physics **11**, 41 (2018).

[19] D. Mardanbegi *et al.*, Vision Res. **143**, 1 (2018).

[20] M. Nyström, I. Hooge, and R. Andersson, Vision Res. **121**, 95 (2016).

[21] D. Kimmel, D. Mammo, and W. Newsome, Front. Behav. Neurosci. **6**, 49 (2012).
[22] J. Otero-Millan, X. G. Troncoso, S. L. Macknik, I. Serrano-Pedraza, and S. Martinez-Conde, J. Vision **8**, 21 (2008).
[23] S. Martinez-Conde, J. Otero-Millan, and S. L. Macknik, Nat. Rev. **14**, 83 (2013).
[24] R. H. S. Carpenter, *Movements of the Eyes* (Pion, UK, 1988).
[25] M. Abramowitz and I. A. Stegun, *Handbook of Mathematical Functions* (Dover, New York, 1965); 10th ed. (1972).
[26] A. Erdelyi, W. Magnus, F. Oberhettinger, and F. G. Tricomi, *Higher Trascendental Functions* (McGraw-Hill, New York, 1953), Vols. I, II, and III.
[27] H. M. Srivastava and H. L. Manocha, *A Treatise on Generating Functions* (Ellis Horwood, Chichester, 1978).
[28] M. R. Harwood and C. M. Harris, Ann. N.Y. Acad. Sci. **956**, 414 (2002).
[29] C. M. Harris, J. Wallman, and C. A. Scudder, J. Neurophysiol. **63**, 877 (1990).